

Differentiable simulations for particle tracking in accelerators: analysis, benchmarking and optimization

Francisco Huhn* and Francesco M. Velotti†

CERN, Geneva, Switzerland

(Dated: July 14, 2025)

Optimization of beamlines and lattices is a common problem in accelerator physics, which is usually solved with semi-analytical methods and numerical optimization routines. However, these are usually of the gradient-free or finite-differences type, whose computational cost grows quickly with the number of optimization parameters. On the other hand, the cost of gradient-based optimization can scale well with the number of parameters, but only if the computation of the gradient is itself efficient (e.g. not via finite differences, which are inefficient). Recently, there has been an emergence of so-called “differentiable” codes that efficiently provide gradients. Nevertheless, analysis and benchmarking comparisons of these techniques have largely been absent from the literature.

In this work, we develop our own differentiable code^a, via auto-differentiation. We analyze and benchmark differentiability against finite differences in two test cases, a space-charge FODO cell from the literature and a realistic future beamline at CERN. The analyses and benchmarking are done both theoretically and empirically. Finally, we embed the gradient provided by the differentiable code in gradient-based optimization routines and compare with gradient-free methods. This work offers the first such analysis and benchmarking and thus contributes towards the development of more efficient and performant particle accelerators.

Keywords: differentiable simulations, auto-differentiation, gradient-based, optimization

I. INTRODUCTION

Optimization of beamlines or lattices is a common problem in accelerator physics in which one or a handful of objectives is minimized/maximized, potentially subject to constraints, by varying a number of parameters, such as quadrupole strengths, etc. Common objectives are Twiss functions matching [1], beam size minimization (e.g. [2]), beam-distribution tailoring [3], etc. Numerical optimization algorithms, in contrast with manual or grid search, have been successfully applied to efficiently solve these problems (e.g. [2, 4]). These numerical routines can be provided by an external package and paired with a accelerator-physics simulation software or be provided by the simulation tool itself. MAD-X [5] is among the most widely used simulation packages in accelerator physics and provides both gradient-based, via finite differences, and gradient-free, like Simplex [6], optimization routines. More recent tools such as Xsuite [7] provide comparable functionality for lattice tuning. Nevertheless, for tracking-based optimization or for the global design of a lattice (e.g. element count and placement), practitioners predominantly adopt gradient-free methods, as the finite-difference evaluation of derivatives incurs a prohibitive computational cost. However, gradient-free algorithms suffer from the “curse of dimensionality” [8], where the computational cost quickly becomes prohibitive as the number of parameters increases, rendering their application unfeasible in mid- to high-dimensional design spaces[9].

On the other hand, gradient-based algorithms, which make use of the derivative of the objective (and constraints) with respect to the design parameters, in conjunction with the adjoint technique for gradient computation, are computationally efficient – they have been extensively applied in various fields, from fluid mechanics [10, 11], where simulations can range from thousands to hundreds of millions of degrees of freedom, to machine learning [12], where models with up to billions of parameters are optimized. The use of the adjoint technique is critical, as naive computation of the gradient, such as via finite differences, is inefficient, because it suffers from the same curse of dimensionality as gradient-free methods (see Section II A). In this technique, the adjoint system is obtained and used to propagate adjoint vectors backward in time, which allows for an efficient computation of the gradient (see Section II B). Traditionally, the adjoint system would be derived analytically and then numerically implemented in code. However, this approach has several disadvantages, being: i) laborious, as deriving the adjoint system analytically can quickly become unwieldy; ii) error prone, as the mathematical expressions must be manually transposed; iii) cumbersome to maintain, especially in updates (e.g. when a new feature is implemented). Alternatively, one can make use of auto-differentiation (see Section II C, which breaks down all computational operations into a graph of elementary operations, over which applying the chain rule becomes straightforward. This approach suffers from none of the aforementioned issues, but comes at the cost of building the graph, i.e. computational overhead, and storing it, i.e. memory cost. It is this method that has enabled and powered the successful training of large models in the field of machine learning, and is provided by the most popular libraries, such as PyTorch [13], TensorFlow [14], JAX [15], etc.

* francisco.huhn@cern.ch

† francesco.maria.velotti@cern.ch

^a The code used in this paper can be found here.

In accelerator physics, the application of the adjoint technique (be it explicit or via auto-differentiation) is scarce. While new so-called “differentiable” simulation codes have emerged [16–19], they are still far from mainstream in the community. More importantly, use-case examples are often of the tutorial class, i.e. too simple, and comprehensive benchmarking and comparisons of the methods – both qualitative and quantitative – are largely absent from the literature. In fact, the only empirical comparison between finite differences and auto-differentiation is found in a passage in [18], which states that auto-differentiation takes twice as long as (central) finite differences to compute the same gradient. However, a relevant detail absent from the paper, but mentioned in the code repository [20] is that only forward auto-differentiation was implemented. Since the problem has seven parameters and one objective, reverse (i.e. adjoint), not forward, auto-differentiation is likely the optimal method (see Section II B for a discussion on forward vs adjoint). Therefore, to the best of our knowledge, this publication represents the first time-performance benchmarking and comparison between finite differences and auto-differentiation, as well as between gradient-free and gradient-based optimization.

II. GRADIENT COMPUTATION

Before delving into the details of the computation of the gradient, let us define the problem. The beamline is composed of N elements. Starting from the initial state $\mathbf{x}_0 \in \mathbb{R}^{N_p \times 6}$ (if using 6 dimensions for each particle), where N_p is the number of particles, we can track the particles by iterating over the elements, i.e. by sequentially applying the (potentially nonlinear) transfer maps of each element

$$\mathbf{x}_n = \mathbf{f}_n(\mathbf{x}_{n-1}; \mathbf{p}_n) \quad (1)$$

where \mathbf{f}_n is the transfer map and \mathbf{p}_n the vector of parameters of the n -th element. Equation (1) is called the primal and is what is commonly meant by “simulation”.

We wish to minimize the objective

$$L(\mathbf{x}_0, \dots, \mathbf{x}_N; \mathbf{p}_1, \dots, \mathbf{p}_N), \quad (2)$$

which depends on the states, \mathbf{x}_n , and on the parameters, potentially explicitly (e.g. one might wish to add a penalty proportional to magnet strengths), but always implicitly via the states, as $\mathbf{x}_n = \mathbf{g}_n(\mathbf{x}_0; \mathbf{p}_1, \dots, \mathbf{p}_n)$. For simplicity, yet, without loss of generality (generality can be achieved via composition), we will assume going forward that only the first element has parameters, $\mathbf{p}_1 = \mathbf{p} = (p_1 \dots p_m)$, and the objective function only depends on the final state of all the states, i.e. we have $L(\mathbf{x}_N; \mathbf{p})$.

A. Finite Differences

In finite differences (FD), the gradient is computed by computing each partial derivative via a perturbation of

the primal. For example, in the simplest case, forward FD, which approximates derivatives to first order:

$$\frac{\partial L}{\partial p_i} \approx \frac{L(\mathbf{x}_N; p_1, \dots, p_i + \epsilon, \dots, p_m) - L(\mathbf{x}_N; p_1, \dots, p_m)}{\epsilon}. \quad (3)$$

To obtain the whole gradient, i.e. derivatives for all parameters, one must compute m perturbed primals and one unperturbed. In central FD (second order), $2m$ perturbed primals are needed. Generally, denoting the cost of one primal by C_P , the cost of FD is

$$C_{FD} = (am + b)C_P, \quad (4)$$

where the constants a and b depend on the type of FD (e.g. $a = 1, b = 1$ for forward, $a = 2, b = 0$ for central), i.e. the cost of computing the gradient is proportional to the number of parameters and cost of a primal.

B. Differentiation

Alternatively, let us attempt to compute the gradient via calculus

$$\frac{dL}{d\mathbf{p}} = \frac{\partial L}{\partial \mathbf{p}} + \frac{\partial L}{\partial \mathbf{x}_N} \frac{\partial \mathbf{x}_N}{\partial \mathbf{p}}. \quad (5)$$

The first term of the RHS is straightforward to compute. Focusing on the second term, we successively apply the chain rule, obtaining

$$\frac{\partial L}{\partial \mathbf{x}_N} \frac{\partial \mathbf{x}_N}{\partial \mathbf{p}} = \frac{\partial L}{\partial \mathbf{x}_N} \frac{\partial \mathbf{f}_N}{\partial \mathbf{x}} \bigg|_{\mathbf{x}_{N-1}} \dots \frac{\partial \mathbf{f}_1}{\partial \mathbf{p}} \bigg|_{\mathbf{x}_0}, \quad (6)$$

where the terms $\partial \mathbf{f}_n / \partial \mathbf{x}$ are the Jacobians of the transfer map of each element. Denoting the dimension of the system D (e.g. $D = 6N_p$), the first term of Eq. (6) is a $1 \times D$ vector. Each of the Jacobians is equivalent to a $D \times D$ matrix. Finally, the last term is a $D \times m$ matrix.

The RHS of Eq. (6) can be computed from right to left or left to right. Right to left is called forward[21] or tangent mode. In this case, we have an $N - 1$ -long series of $D \times D$ by $D \times m$ multiplications, followed by one $1 \times D$ by $D \times m$, resulting in a computational cost of

$$C_C = ((N - 1)D^2 m + Dm) c_{ma}, \quad (7)$$

where c_{ma} is the cost of a scalar multiplication-addition. Left to right is called reverse or adjoint mode. Analogously, we have an $N - 1$ -long series of $1 \times D$ by $D \times D$ multiplications, followed by one $1 \times D$ by $D \times m$, resulting in a complexity of

$$C_C = ((N - 1)D^2 + Dm) c_{ma}. \quad (8)$$

Clearly, from Eqs. (7) and (8), adjoint mode is advantageous as m is increased, since m is multiplied only by D , in contrast with $(N - 1)D^2 + D$ in tangent. This is the case because we are considering the situation of one

objective function and m parameters. If, instead, we had m objective functions and one parameter, the situation would be reversed. When the number of parameters is greater than the number of objectives, one should prefer the adjoint approach; and tangent, otherwise.

Irrespective of the approach, adjoint versus tangent, to calculate the gradient via Eq. (6), the states \mathbf{x}_n are required (i.e. the primal must be computed), as well as the terms $\partial f_n / \partial \mathbf{x}|_{\mathbf{x}_{n-1}}$, necessary to differentiate the transfer maps. Thus, the total cost of the method in terms of the cost of the primal is

$$\frac{C_A}{C_P} = \frac{C_P + C_D + C_C}{C_P}, \quad (9)$$

where C_P , C_D and C_C are the costs of the primal, differentiation and the computation of the chained derivative by multiplication-addition of the chain of the partial derivatives in adjoint mode. The cost of differentiation, C_D , is $O(C_P)$ [22], which we write, foregoing any dominated terms, as

$$C_D = \kappa_{dp} C_P. \quad (10)$$

The relative cost of computing the chained derivative, C_C/C_P , depends on the problem, i.e. the primal, and the approach, tangent or adjoint. For example, for a full linear primal, $C_P = O(ND^2)$, whereas, generally, nonlinearities will introduce higher computational complexity. Equation (8) for C_C and Eq. (10) can be substituted in Eq. (9) to obtain the total cost

$$\frac{C_A}{C_P} = 1 + \kappa_{dp} + \kappa_{sp} + \kappa_{mp} m, \quad (11)$$

where $\kappa_{sp} = c_{ma}(N-1)D^2/C_P$ and $\kappa_{mp} = c_{ma}D/C_P$. Therefore, while, strictly speaking, the adjoint's cost scales linearly with the number of parameters (similarly to FD), the linear coefficient, κ_{mp} , is small to negligible. Additionally, $\kappa_{sp} \rightarrow 0$ as the computational complexity of the primal increases. For example, even with a, computationally simple, linear primal, $\kappa_{mp} = c_{ma}D/(c_{ma}ND^2) = 1/(ND)$ and $\kappa_{sp} = c_{ma}(N-1)/(c_{ma}N) = (N-1)/N$.

This highlights the big advantage of the adjoint method: computing the gradient on one parameter costs approximately the same as on any number of parameters[23], which contrasts with FD, where the linear coefficient is $O(1)$. For m objective functions and one parameter, analysis of the tangent approach, i.e. forward propagation, results in similar expressions.

C. Auto-differentiation

While one may derive the analytical expressions of $\partial \mathbf{f}_n / \partial \mathbf{x}_n$ and other terms, as mentioned in Section I, this is laborious, error prone and hard to maintain. Instead, auto-differentiation (AD) can be used. In AD, complex computations, e.g. the primal, are broken down into a directed acyclic graph of elementary operations, whose

derivatives are known, over which the chain rule can be applied successively. An example of reverse AD (AD-REV) for a thin-sextupole kick is given in Appendix A 1 and a cost analysis of the method is given in Appendix A 2.

Auto-differentiation found great applicability and success in machine learning [24], with the most popular libraries (e.g. PyTorch [13], TensorFlow [14], JAX [15]) providing it as an out-of-the-box feature. In the majority of cases, very little setup is needed – one programs the primal as a function and then calls the auto-differentiation function (tangent of adjoint) on it. Moreover, these libraries provide GPU support, enabling the study of more computationally-demanding cases. While PyTorch has been framework of choice for new differentiable codes [16, 17], we implement ours[25] on top of JAX, which is designed for high-performance numerical computing and provides a NumPy-style API.

D. Computational time vs complexity

While it should be clear that above a certain number of parameters or primal computational complexity, (auto-)differentiation should be advantageous with respect to finite differences, it is not clear what this number is. Analyzing the expressions for the computational cost of each method would suggest it is small. However, the situation is complicated by parallelization. For example, the different perturbed primals of finite differences can be straightforwardly run in parallel. Doing the same for the adjoint is significantly harder. This is where the distinction between computational time and complexity becomes important. In the end, practitioners are interested in shorter computational times, not necessarily complexity. Thus, it may turn out that, despite having higher complexity, finite differences may be faster than the adjoint. Hence the necessity for the kind of benchmarking and comparison done in this work. It follows thus that the relationship between computation time and complexity is strongly dependent on the interplay between the problem (system size, density, etc.), the method/numerics (FD, AD and their implementation) and the machine (e.g. CPU, GPU, memory, etc.). Our tests were run on a machine with Intel Xeon Silver 4110 CPU, 16 GB RAM, Tesla V100 with 32 GB VRAM, which we believe is representative of those available to accelerator-physics practitioners.

III. PROBLEMS AND RESULTS

A. FODO with space charge

1. Single cell

This case is taken from [18]. It is a 6D tracking problem of 5000 particles over a FODO cell with space-charge effects[26]. Following the reference, each of the drifts is sliced into segments of 0.05 m and the quadrupoles

are sliced into segments of 0.025 m. The drift segments are integrated via drift-kick-drift, with the kick due to space-charge effects. The quadrupole segments are similarly halved, with space-charge kick applied between the halves, with each half being further subdivided into 20 sub-segments, with each sub-segment being integrated via the 7-step Yoshida integrator (fourth order). The objective functions are the horizontal and vertical emittances. There are seven parameters, five lengths (one per each of the three drifts and one per each of the two quadrupoles) plus two strengths (one per quadrupole).

We compare the values of the gradients obtained via AD (adjoint) and FD (central FD with step of 10^{-6} [18]). Figure 1 shows great agreement between the two methods and the values are also very similar[27] to those found in [18]. Figure 2 shows the execution time for each method

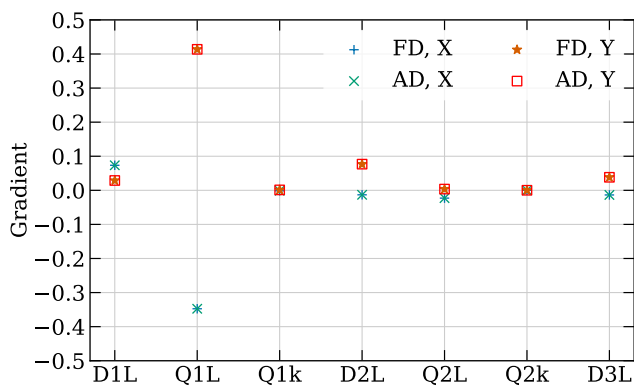


FIG. 1: Gradients of horizontal (X) and vertical (Y) emittances, via auto-differentiation (AD) and finite differences (FD).

FD, AD-FWD, AD-REV, as well as the primal, on both CPU and GPU. On CPU, as the computational complexity (due to the number of particles) increases, the computational times increase. However, normalizing by the cost of a primal (i.e. of one simulation), we can see that AD-REV costs the equivalent of 5 primals, while FD costs close to 3 times more. On the other hand, AD-FWD costs only slightly less than FD, which is not unsurprising given the low number of parameters. Notice, however, that this is in stark contrast with the findings in [18] that FD is twice as fast as AD-FWD. On GPU, however, there is a surprising reversal: AD-REV becomes the least-performing method for the majority of cases ($N_p \leq 9000$) and is only marginally faster than FD at $N_p = 10000$. Nevertheless, auto-differentiation still comes ahead with FWD. The reason for these, at first, surprising, results, is alluded to in Section II D. GPUs possess great parallel processing power, which lends itself greatly to FD and AD-FWD, as both can take advantage of this capability due to their embarrassingly-parallel nature, and not so much to AD-REV. Despite needing more operations, in FD and AD-FWD, these can be executed in parallel. An analysis of time versus complexity in the following

section (Fig. 5) effectively demonstrates this. This is an advantage that should subside with increasing problem complexity – indeed, at $N_p = 10000$, we already observe a reversal in the relative performance of FD vs AD-REV.

2. Multiple cells

We slightly modify the FODO cell of the previous section. To slightly reduce the computational cost of each cell, we reduce the number of integration steps of a half slice from 20 to 5. To avoid two consecutive drifts, we double the length of the first drift and remove the last drift. Taking this modified cell, we make a beamline of up to 5 cells. Thus, we not only add computational complexity to the problem, similarly to adding more particles, but also increase the number of parameters. With this increase, the performance gap between FD and AD should become larger (see Section II B). The results for CPU (Fig. 3) show that, as in the previous section, AD-REV is 3 times faster than FD for 1 cell, but for 5 cells it is 15 times faster. This is not surprising, since the computational cost of AD-REV is practically constant in primal terms, whereas that of FD increases linearly with the number of parameters. On the other hand, if the code is executed on GPU (Fig. 4a), we can see that FD is faster than AD-REV for cases of low number of cells and low number of particles. Once again, this shows the potential of FD to take advantage of parallelization in “small” problems. However, in these cases, AD-FWD is even faster than FD (Fig. 4b). The computational time vs complexity distinction can be clearly seen in Fig. 5, where time is plotted versus an estimate of the number of operations[28]. For the same number of operations, the AD-REV takes longer than FD and AD-FWD.

In essence, for the cases analyzed, AD-REV is generally faster than FD, both on CPU and GPU. When solving small cases on GPU, AD-REV may be slower than FD, but AD-FWD is still faster than FD, which means that auto-differentiation is more efficient than finite differences in all cases tested.

B. Realistic beamline

To obtain a more realistic estimate of each method’s performance, we have chosen a high-energy beamline so that collective effects can be safely neglected[29], incorporating both sextupole and octupole magnets. This is the 150 MeV electron transfer line now being designed for the next phase of the CERN AWAKE experiment; it is designed to deliver micrometer-scale transverse beam sizes at the plasma injection point for subsequent acceleration [2].

Unlike the problem in Section III A, there are no collective effects. In this case, far more typical, each particle evolves independently – the joint system (i.e. system of all particles) is a block-diagonal system, each block

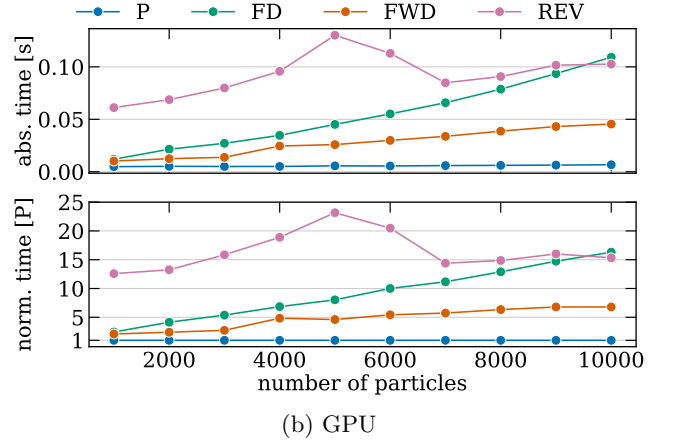
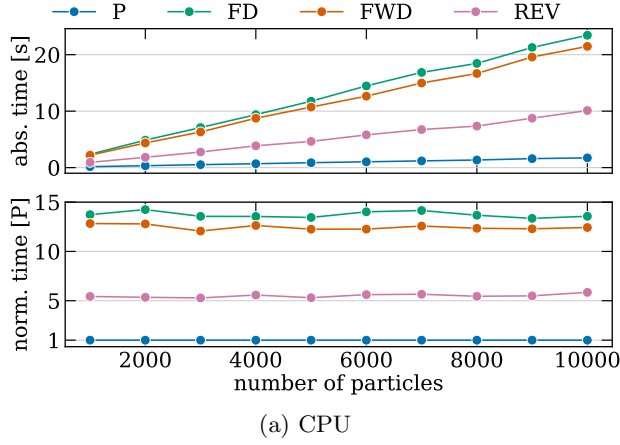


FIG. 2: Execution times of primal (P), finite differences (FD), adjoint auto-differentiation (REV), tangent auto-differentiation (FWD). Top panels: absolute time; bottom panels: normalized by primal time.

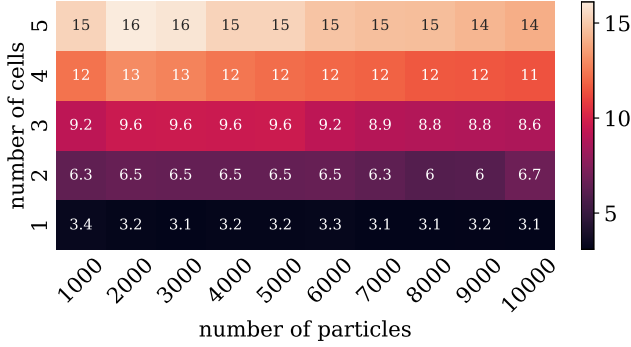


FIG. 3: Ratio of execution times: FD over AD-REV – CPU.

corresponding to a particle. The beamline (Fig. 6) is composed of: drifts, sector bends, quadrupoles, sextupoles and octupoles, for a total of 39 elements, resulting in 58 parameters (Table I)[30]. With exception of sector bends, all magnets are modeled as drift-kick-drift. For simplicity, we do not implement fringe fields or particle losses.

Element Type	Parameters	NoE ^a	NoP ^b
drift	length	20	20
sector bend	length, angle	2	4
quadrupole	length, strength	8	16
sextupole	length, strength	6	12
octupole	length, strength	3	6
Total		39	58

^a Number of Elements

^b Number of Parameters

TABLE I: Elements of the AWAKE line.

The objective is to minimize

$$\frac{1}{N_p} \sum_{i=1}^{N_p} (x_i^2 + y_i^2), \quad (12)$$

i.e. the mean distance from the center. Figure 7 shows that the sensitivities of Eq. (12) with respect to beamline parameters obtained via auto-differentiation match those computed using (central) finite differences.

Having validated the numerical values, we now compare the time efficiencies of these methods. Figure 8 shows the execution times, absolute and normalized by the time to run one simulation, i.e. one primal. On CPU, AD-REV is one order of magnitude faster than FD. AD-FWD is also significantly slower than AD-REV, but still faster than FD. On GPU, AD-FWD is the fastest method for $N_p \leq 4000$ particles, above which it is AD-REV. On the other hand, FD is always slower than either AD-FWD or AD-REV and is the slowest for $N_p \geq 3000$. The speedup from using auto-differentiation ranges from marginal at $N_p = 1000$ to a factor of 3 at the upper end of range of particles tested. We remark that the lower computational complexity of the primal (no collective effects and lower number of slices) with respect to the cases in Section III A[31] is a factor that benefits FD, relative to AD (see Section II B). Nevertheless, we observe the opposite: the overperformance of AD over FD increases. The reason is that the number of parameters increases from ≤ 30 to 59. This comparison highlights the two positive factors of overperformance of AD with respect to FD: computational complexity of the primal and number of parameters.

1. Optimization

Even if AD is more efficient than FD at computing the gradient, it does not necessarily follow that gradient-based optimization with AD is more efficient than gradient-free

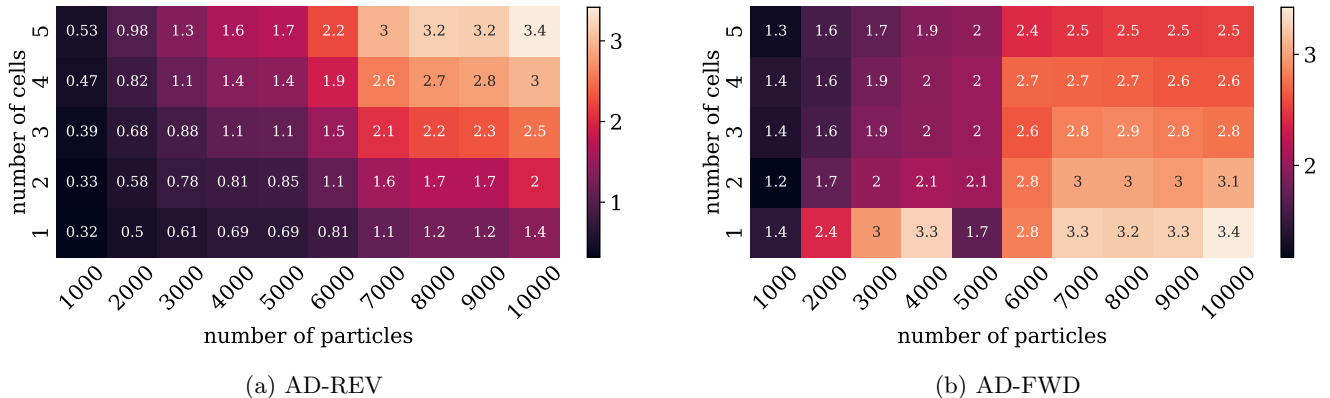


FIG. 4: Ratio of execution times: FD over AD – GPU.

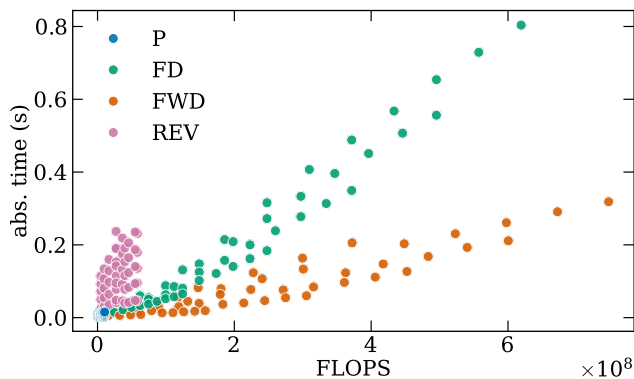


FIG. 5: Execution time versus number of operations

methods. Therefore, we compare gradient-based methods, SLSQP [32] and L-BFGS-B [33], with one of the most common and performant gradient-free methods, Nelder-Mead [6] (it dominated the gradient-free methods we tested). For a balance between a more realistic scenario (e.g. no nonsensical negative-length drifts) with simplicity, we bound the parameters to $\pm 50\%$ of their initial values. Figure 9 shows the evolution of each of the optimizations over time. It shows that both gradient-based methods achieve their optima faster than the gradient-free method and that their optima are better (lower objective function). Figure 10 shows the initial distribution and each of the three final distributions, showing the noticeable improvement in the objective.

IV. CONCLUSION

We analyzed, both theoretically and empirically, the efficiency of finite differences versus auto-differentiation, concluding that AD-REV is almost always faster than FD. The speedup can range from marginal to orders of magnitude and depends on the physical problem and the

computational machine. It is more significant on CPU than on GPU, owing to the latter's parallel processing power, of which FD can better take advantage. Notwithstanding, even in cases where FD is faster than AD-REV, it is slower than AD-FWD. Moreover, we embedded the sensitivities calculated via AD-REV in a gradient-based optimizer to solve a parameter-bounded problem, and compared that with a common gradient-free method, finding that the gradient-based approach is faster and reaches a better minimum.

This work shows that differentiable simulations present significant advantages in beam-line optimization and have the potential to improve accelerator design in the search for higher and more robust performance.

Appendix A: Auto-differentiation

1. Example

As explained in Section II C, auto-differentiation represents the numerous computational operations of a computationally-complex function as directed acyclic graph (DAG) of, usually unary or binary, elementary operations. Figure 11 shows such a graph for the horizontal kick of a thin sextupole, which is given by the expression

$$\Delta x' = \frac{k_2}{2}(y^2 - x^2), \quad (\text{A1})$$

where k_2 is the sextupole strength, and x and y are the horizontal and vertical positions. From left to right and in depth-first order, the expression can be broken down

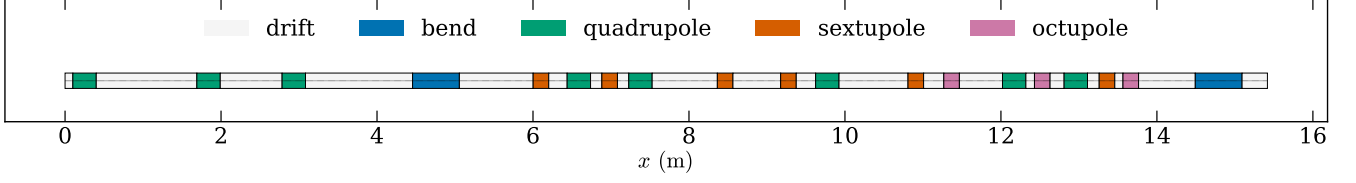


FIG. 6: AWAKE line

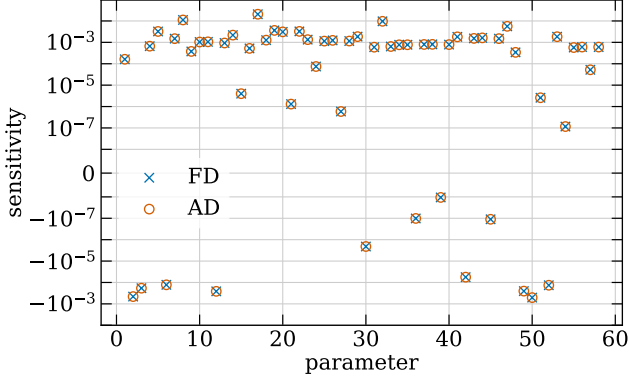


FIG. 7: Sensitivity of the objective function (Eq. (12)) with respect to beamline parameters, via auto-differentiation (AD) and finite differences (FD).

into:

$$u_1 = k_2 \quad (\text{A2})$$

$$u_2 = 2 \quad (\text{A3})$$

$$u_3 = u_1/u_2 \quad (\text{A4})$$

$$u_4 = y \quad (\text{A5})$$

$$u_5 = u_4^2 \quad (\text{A6})$$

$$u_6 = x \quad (\text{A7})$$

$$u_7 = u_6^2 \quad (\text{A8})$$

$$u_8 = u_5 - u_7 \quad (\text{A9})$$

$$u_9 = u_3 \times u_8 \quad (\text{A10})$$

$$\Delta x' = u_9 \quad (\text{A11})$$

This is shown in Fig. 11a. With given values for k_2 , x and y , the graph can be traversed and $\Delta x'$ can be obtained at u_9 . Then, starting from the top-most node, i.e. the quantity we wish to differentiate, reversed traversal is executed. At every node with result u_i , the partial derivative is computed with respect to each argument (i.e. for each child edge), a value that is then multiplied by the chained derivative to produce the chained derivative of the argument node, i.e. $\partial u_9/\partial u_i$. For example, the partial derivative of u_5 with respect to its argument, u_4 , is $\partial u_5/\partial u_4 = 2u_4$, which is then multiplied by the chained derivative,

$$u_3 \cdot 2u_4 = \left(\frac{\partial u_9}{\partial u_8} \frac{\partial u_8}{\partial u_5} \right) \cdot \frac{\partial u_5}{\partial u_4} = \frac{\partial u_9}{\partial u_4}. \quad (\text{A12})$$

Figures 11b and 11c show these steps. The steps are shown in separate figures for clarity. They are applied in succession at each edge of the graph. Finally, at the leaves, the expressions for the chained gradients are

$$\begin{pmatrix} \frac{\partial u_9}{\partial k_2} \\ \frac{\partial u_9}{\partial x} \\ \frac{\partial u_9}{\partial y} \end{pmatrix} = \begin{pmatrix} u_2 u_8 \\ -u_3 u_6 \\ u_3 u_4 \end{pmatrix} = \begin{pmatrix} \frac{1}{2}(y^2 - x^2) \\ -k_2 x \\ k_2 y \end{pmatrix}, \quad (\text{A13})$$

which match the analytical differentiation of Eq. (A12).

2. Cost analysis

The AD framework also presents an alternative way to derive the computational cost of differentiation. Here, as in most computational machines, we consider a DAG of unary or binary operations, although the same could be done for any arity. The first step is to compute the primal via a forward pass, which costs

$$C_P = \sum_{i=1}^n c_p^{(i)}, \quad (\text{A14})$$

where $c_p^{(i)}$ is the cost of the operation of node i and n is the number of non-leaf nodes. The second step is backpropagation, where, for each non-leaf node, one must compute the derivative with respect to each of its children, multiply by the chained derivative and accumulate in the child node. The derivatives cost

$$C_D = \sum_{i=1}^n \left(c_d^{(i,1)} + c_d^{(i,2)} \right) \quad (\text{A15})$$

$$= \sum_{i=1}^n \frac{c_d^{(i,1)} + c_d^{(i,2)}}{c_p^{(i)}} c_p^{(i)} \quad (\text{A16})$$

$$= \sum_{i=1}^n \kappa_{dp}^{(i)} c_p^{(i)} \quad (\text{A17})$$

$$= \kappa_{dp} \sum_{i=1}^n c_p^{(i)} \quad (\text{A18})$$

$$= \kappa_{dp} C_P, \quad (\text{A19})$$

where $c_d^{(i,j)}$ is the cost of computing the derivative of node i with respect to its j -th child – while the ratio κ_{dp} depends on the operations of the primal, usually,

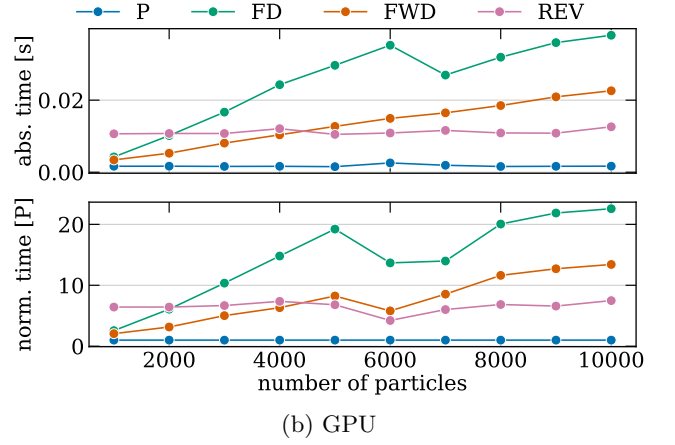
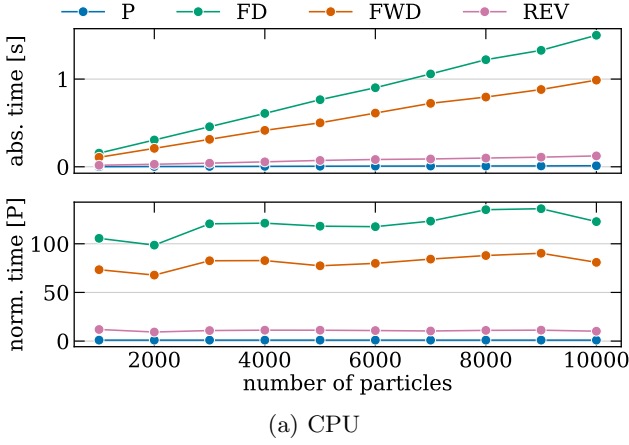


FIG. 8: AWAKE line – execution times.

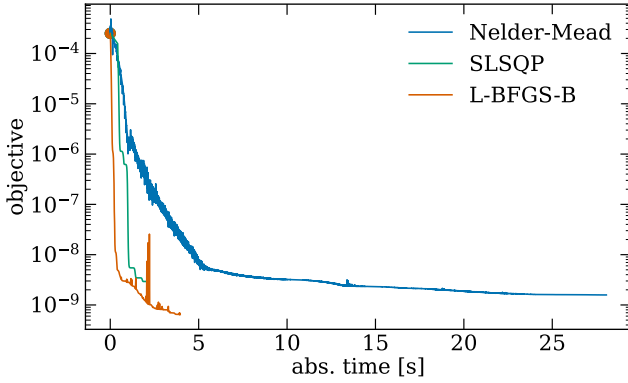


FIG. 9: Objective versus time for each of the methods.

the derivative has a similar cost to the function itself (e.g. $\sin \mapsto \cos$), i.e. normally $\kappa_{dp} \sim O(1)$. The computation of the accumulated chained derivative costs one multiplication and addition per edge, i.e.

$$C_C = n_e c_{ma} \quad (A20)$$

$$= \left(\sum_{i=1}^n l_{\text{node}}^{(i)} + \sum_{i=1}^m l_{\text{param}}^{(i)} \right) c_{ma} \quad (A21)$$

$$= (\bar{l}_{\text{node}} n + \bar{l}_{\text{param}} m) c_{ma} \quad (A22)$$

$$= \frac{(\bar{l}_{\text{node}} n + \bar{l}_{\text{param}} m) c_{ma}}{C_P} C_P \quad (A23)$$

$$= (\kappa_{sp} + \kappa_{mp} m) C_P, \quad (A24)$$

where n_e is the number of edges, $l_{\text{node}}^{(i)}$ and $l_{\text{param}}^{(i)}$ are the number of parent edges of the internal nodes and the parameter nodes, and the bar denoting average. Adding up the three costs gives

$$\frac{C_A}{C_P} = \frac{C_P + C_D + C_C}{C_P} = 1 + \kappa_{dp} + \kappa_{sp} + \kappa_{mp} m, \quad (A25)$$

which coincides with Eq. (11).

Appendix B: Accelerator physics vs machine learning

A beamline can be seen as a neural network, where each beamline element is a network layer. Thus, it would seem that the remarkable efficiency of AD-REV in machine learning should transfer to beamline optimization. This is, alas, not necessarily the case. Comparing networks, those of machine learning are shallow (even in deep learning) relative to those in beamlines. At the same time, they are wider and more connected. For example, while one dense neural network layer may add tens to thousands of parameters, a quadrupole only adds two. Similarly, the dense layer adds tens to thousands of nonlinearities, while a sextupole only adds two.[34] For a beamline to have a significant number of parameters, such that using AD-REV is advantageous, it must be somewhat deep. Concomitantly, depth may be disadvantageous, as AD-REV requires keeping the graph of the operations of the primal in memory. This suggests that a jump in application of AD-REV from beamline to lattice, wherein hundreds to thousands of turns are executed, may not be as straightforward as it might seem at first sight – the depth of the DAG would be proportional to the lattice size and the number of turns. In this case, potentially, the judicious choice might be AD-FWD, where the chained derivatives are computed and brought up along with the primal, foregoing the need to keep the graph in memory. Moreover, the results on GPU of Sections III A and III B suggest that the considerable theoretical disadvantage of forward mode with respect to reverse may not be as significant in practice and may therefore not be an impediment to the application of AD-FWD.

In essence, while we show theoretically and empirically that AD-REV (and AD-FWD) can and is usually be faster FD, it should not be assumed that, because it generally does so in other fields, it should do as well in accelerator physics – while the methodology is similar, the specifics are not.

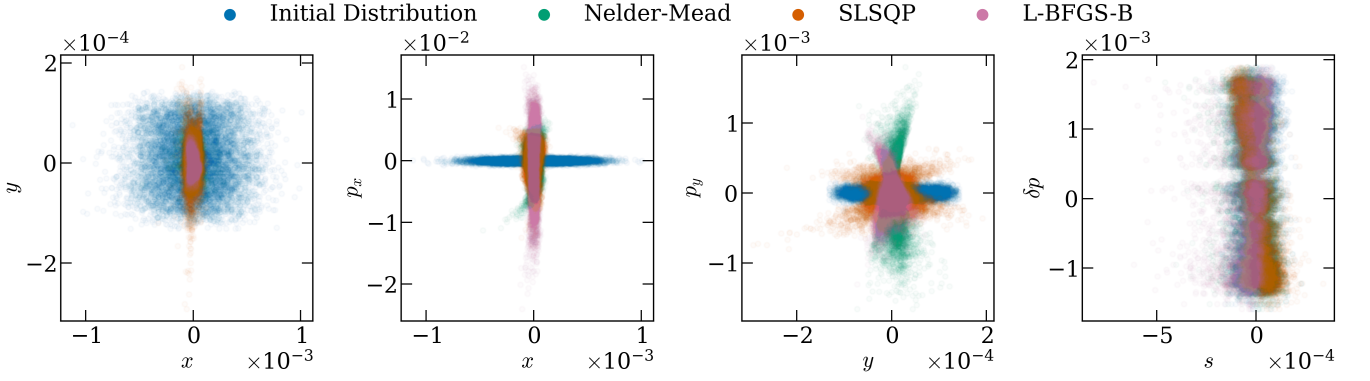


FIG. 10: Initial distribution and final distributions for each of the methods. The final distribution of the initial design is not shown because it is much larger than the plotting ranges.

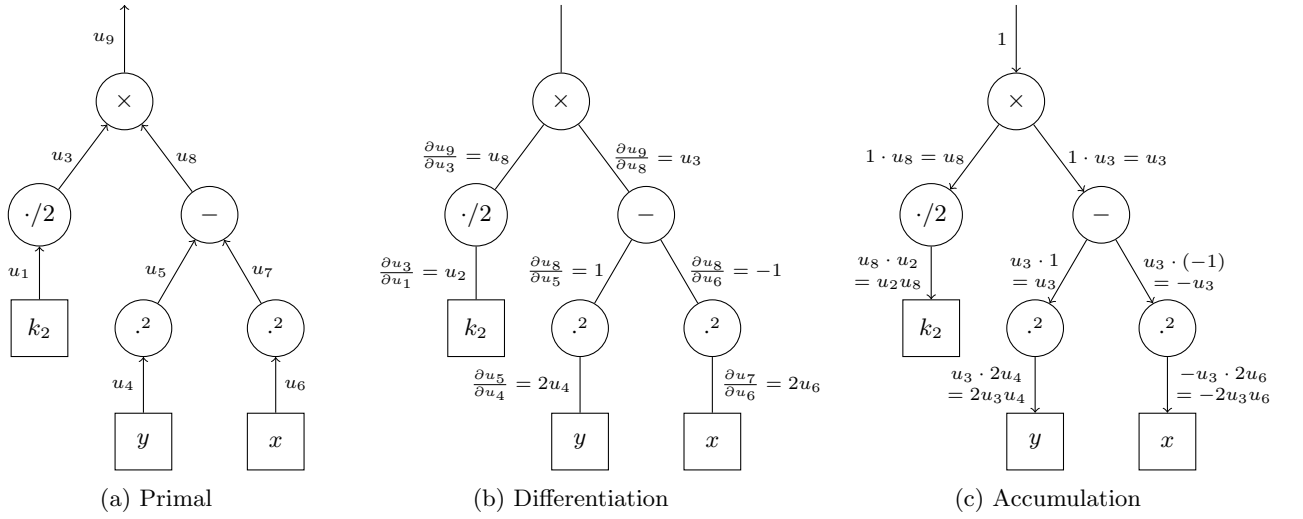


FIG. 11: Reverse auto-differentiation of the horizontal kick of a thin sextupole, $\frac{k_2}{2}(y^2 - x^2)$. For simplicity, $u_2 = 2$, the second argument in $k_2/2$, has been merged into the operation node.

-
- [1] C. Iselin, The mad program, in *Computing in Accelerator Design and Operation*, edited by W. Busse and R. Zelazny (Springer Berlin Heidelberg, Berlin, Heidelberg, 1984).
- [2] R. Ramjiawan, S. Döbert, J. Farmer, E. Gschwendtner, F. M. Velotti, L. Verra, G. Z. Della Porta, V. Bencini, and P. N. Burrows, Design and operation of transfer lines for plasma wakefield accelerators using numerical optimizers, *Phys. Rev. Accel. Beams* **25**, 101602 (2022).
- [3] M. Remta, F. Velotti, F. Huhn, P. Arrutia Sota, and Y. Duthel, Towards tailored beam distributions for fixed target experiments at cern, in *Proc. 16th International Particle Accelerator Conference, IPAC'25 - 16th International Particle Accelerator Conference No. 16* (JACoW Publishing, Geneva, Switzerland, 2025) pp. 967–970.
- [4] L. Yang, D. Robin, F. Sannibale, C. Steier, and W. Wan, Global optimization of an accelerator lattice using multiobjective genetic algorithms, *Nuclear Instruments and Methods in Physics Research Section A: Accelerators, Spectrometers, Detectors and Associated Equipment* **609**, 50 (2009).
- [5] L. Deniau et al., MethodicalAcceleratorDesign/MAD-X: 5.09.01 (2023).
- [6] J. A. Nelder and R. Mead, A simplex method for function minimization, *The Computer Journal* **7**, 308 (1965).
- [7] G. Iadarola et al., Xsuite: An Integrated Beam Physics Simulation Framework, *JACoW HB2023*, TUA2I1 (2024), arXiv:2310.00317 [physics.acc-ph].
- [8] N. Hansen, A. Auger, R. Ros, S. Finck, and P. Pošík, Comparing results of 31 algorithms from the black-box optimization benchmarking bbob-2009 (Association for Computing Machinery, New York, NY, USA, 2010) p. 1689–1696.
- [9] What is considered mid and high dimensional depends on the problem and the computational resources available.

- [10] A. Jameson, Aerodynamic design via control theory, *Journal of Scientific Computing* **3**, 233 (1988).
- [11] L. Magri, Adjoint methods as design tools in thermoacoustics, *Applied Mechanics Reviews* **71**, 020801 (2019).
- [12] Our World in Data, Computation used to train notable ai systems, by domain (2024).
- [13] J. Ansel, E. Yang, H. He, N. Gimelshein, A. Jain, M. Voznesensky, B. Bao, P. Bell, D. Berard, E. Burovski, G. Chauhan, A. Chourdia, W. Constable, A. Desmaison, Z. DeVito, E. Ellison, W. Feng, J. Gong, M. Gschwind, B. Hirsh, S. Huang, K. Kalambarkar, L. Kirsch, M. Lazos, M. Lezcano, Y. Liang, J. Liang, Y. Lu, C. K. Luk, B. Maher, Y. Pan, C. Puhersch, M. Reso, M. Saroufim, M. Y. Siraichi, H. Suk, S. Zhang, M. Suo, P. Tillet, X. Zhao, E. Wang, K. Zhou, R. Zou, X. Wang, A. Mathews, W. Wen, G. Chanan, P. Wu, and S. Chintala, *PyTorch 2: Faster Machine Learning Through Dynamic Python Bytecode Transformation and Graph Compilation* (Association for Computing Machinery, New York, NY, USA, 2024) p. 929–947.
- [14] M. Abadi, A. Agarwal, P. Barham, E. Brevdo, Z. Chen, C. Citro, G. S. Corrado, A. Davis, J. Dean, M. Devin, S. Ghemawat, I. Goodfellow, A. Harp, G. Irving, M. Isard, R. Jozefowicz, Y. Jia, L. Kaiser, M. Kudlur, J. Levenberg, D. Mané, M. Schuster, R. Monga, S. Moore, D. Murray, C. Olah, J. Shlens, B. Steiner, I. Sutskever, K. Talwar, P. Tucker, V. Vanhoucke, V. Vasudevan, F. Viégas, O. Vinyals, P. Warden, M. Wattenberg, M. Wicke, Y. Yu, and X. Zheng, *TensorFlow, Large-scale machine learning on heterogeneous systems* (2015).
- [15] J. Bradbury, R. Frostig, P. Hawkins, M. J. Johnson, C. Leary, D. Maclaurin, G. Necula, A. Paszke, J. VanderPlas, S. Wanderman-Milne, and Q. Zhang, *JAX: composable transformations of Python+NumPy programs* (2025).
- [16] J. Gonzalez-Aguilera, Y.-K. Kim, R. Roussel, A. Edelen, and C. Mayes, Towards fully differentiable accelerator modeling, in *Proc. 14th International Particle Accelerator Conference, IPAC'23 - 14th International Particle Accelerator Conference No. 14* (JACoW Publishing, Geneva, Switzerland, 2023) pp. 2797–2800.
- [17] J. Kaiser, C. Xu, A. Eichler, and A. Santamaria Garcia, Bridging the gap between machine learning and particle accelerator physics with high-speed, differentiable simulations, *Phys. Rev. Accel. Beams* **27**, 054601 (2024).
- [18] J. Wan, H. Alamprese, C. Ratcliff, J. Qiang, and Y. Hao, *JuTrack: a Julia package for auto-differentiable accelerator modeling and particle tracking* (2024), arXiv:2409.20522 [physics.acc-ph].
- [19] L. Deniau, *Mad-ng, a standalone multiplatform tool for linear and non-linear optics design and optimisation* (2025), arXiv:2412.16006 [cs.CE].
- [20] J. Wan, H. Alamprese, C. Ratcliff, J. Qiang, and Y. Hao, *JuTrack code repository* (2025), Accessed: 2025-06-01.
- [21] Not to be confused with forward FD, which is unrelated.
- [22] For example, if the primal is $f(x, y) = xy$, then $\partial_{\mathbf{p}} f = y \partial_{\mathbf{p}} x + x \partial_{\mathbf{p}} y$ is y and x , i.e. $C_D = 2C_P$.
- [23] Practical limitations, like memory, aside.
- [24] A. G. Baydin, B. A. Pearlmutter, A. A. Radul, and J. M. Siskind, Automatic differentiation in machine learning: a survey, *Journal of Machine Learning Research* **18**, 1 (2018).
- [25] The code used in this paper can be found here.
- [26] Details can be found in the reference.
- [27] The reason for the slight discrepancies is unknown.
- [28] This estimate is obtained via the `func.lower(x).compile().cost.analysis()` method in JAX.
- [29] Coherent synchrotron radiation is the only effect that could be considered but for the purpose of this paper, it was considered negligible.
- [30] The order of the elements and the values of the parameters of the initial design can be found in the project's repository.
- [31] Confirmed by the primals' execution times (see Fig. 2a vs Fig. 8a).
- [32] D. Kraft, Algorithm 733: Tomp–fortran modules for optimal control calculations, *ACM Transactions on Mathematical Software* **20**, 262–281 (1994).
- [33] C. Zhu, R. H. Byrd, P. Lu, and J. Nocedal, Algorithm 778: L-bfgs-b: Fortran subroutines for large-scale bound-constrained optimization, *ACM Trans. Math. Softw.* **23**, 550–560 (1997).
- [34] It is perhaps then not surprising that one of the few publications [35] on application of AD to beamlines is on optimizing a neural network that generates the initial distribution, and not on optimizing the beam-line elements.
- [35] R. Roussel, J. P. Gonzalez-Aguilera, E. Wisniewski, A. Ody, W. Liu, J. Power, Y.-K. Kim, and A. Edelen, Efficient six-dimensional phase space reconstructions from experimental measurements using generative machine learning, *Phys. Rev. Accel. Beams* **27**, 094601 (2024).